MEASUREMENTS OF LAMINAR BURNING VELOCITIES AND FLAME STABILITY ANALYSIS OF BIOMASS DERIVED GAS–AIR PREMIXED FLAMES

Won Sik Song*, Tran Manh Vu*, Jeong Park*, Oh Boong Kwon*, Hyun Seok You, Jin Han Yun*****

jeongpark@pknu.ac.kr

*School of Mechanical Engineering, Pukyong National University, San 100, Yongdang-dong, Nam-gu, Busan 608-739, Korea

**New Energy & Environmental Team, R&D Center, Korea Gas Corporation, 638-1, Il-dong, Sangrock-gu, Ansan 426-860, Korea

***Environment & Energy Research Division, Korea Institute of Machinery and Materials, 171 Jang-dong, Yuseong-gu, Daejeon 305-343, Korea

Abstract

Three biomass derived gases (BDGs, named GG-H, GG-L and GG-V), which are derived from industry facilities and can be useful for reducing CO_2 and the application to combustors, are studied and examined for some basic flame characteristics such as unstretched laminar burning velocity, Markstein length, and cell formation over the entire flame surface. Experiments were conducted in a constant pressure combustion chamber using a schlieren system. A better agreement between the measured and predicted unstretched laminar burning velocities is obtained using a suggested reaction mechanism modified from the GRI-Mech 3.0 mechanism. Additionally, cell formations on flame surfaces of the three mixtures were also analyzed and compared using high-speed schlieren images. It is shown that the GG-H–air flames and the GG-L–air flames have similar flame wrinkled surfaces, while the GG-V–air flames shows a stronger cellularity behavior. The effects of each fuel component in mixtures to cellularity are also evaluated by varying the concentration of each fuel in the reactant mixtures. The cellular instability is promoted (diminished) with hydrogen enrichment (methane addition); meanwhile the similar behavior is obtained for carbon monoxide addition.

Introduction

In recent years, for the purposes of reducing of CO_2 emissions during combustion of fossil fuels and removing of wastes due to environmental and health concerns, biomass derived gas (BDG) has been widely used to replace fossil fuels in combustion engines. The most serious barrier in designing combustion engines using BDGs arises from a large variety of compositions produced from various biomass sources and different techniques. BDGs mainly compose of H_2, CO, CH_4, CO_2, N_2, and can occasionally contain a small amount of higher hydrocarbons [1]. Because of the small lower heating value (LHV) of BDGs, they can ordinary be burned together with natural gas to achieve a higher efficiency of internal combustion engine [2].

In literature, there have been a lot of reports on the fundamental characteristics of pure fuel premixed flames. So far, most studies related to biomass have been rather limited to processes technologies such as gasification and pyrolysis [3–5]. It is rather surprising that the flame characteristics of BDGs flames have not been yet understood thoroughly. The deep understanding in combustion behaviors of BDGs–air flames is very important in designing of combustion devices, validating and developing the chemical kinetic mechanisms, as well as predicting the performance and emission of combustion systems. In this work, three BDGs namely GG-H, GG-L and GG-V which are derived from industry facilities and can be useful

Table 1. Compositions of biomass derived gases studied in the measurements.

BDGs	CO	CO_2	H_2	CH_4	N_2	Biomass	Ref.
GG-H	0.355	0.27	0.287	0.065	0.023	Cellulose	[3]
GG-L	0.2792	0.3011	0.3539	0.0436	0.0222	Pine wood	[4]
GG-V	0.197	0.06	0.591	0.115	0.037	Crude glycerol	[5]

for reducing CO_2 and the application to combustion devices [2], are studied and examined for some basic flame characteristics such as unstretched laminar burning velocity, Markstein length, and cell formation over the entire flame surface. The GG-H represents the gasification gas reported by Hanaoka et al. [3], the GG-L denotes the gasification gas given by Lv et al. [4], and the GG-V is the gasification gas studied by Valliyappan et al. [5]. The compositions of the three BDGs are listed in Table 1.

The most important parameter in designing premixed combustion engines is laminar burning velocity, in that it determines the structure and the flame stability. The behavior of cell formation in premixed flames is another important factor in the side of increasing the flame speed and leading to the engine knock. The cellular instabilities in premixed flames can result from body-force, diffusive-thermal and hydrodynamic effects [6]. The diffusive-thermal effect is caused by the non-similar diffusion of mass versus heat and has a destabilizing influence for Lewis numbers of the deficient reactant lower than unity. The hydrodynamic effect is caused by the thermal expansion through the flame front and is the most essential factor in the flame instability [7]. To clarify the flame characteristics of the BDGs–air mixtures, this study focuses on measurements of the laminar burning velocities and Markstein lengths for a wide range of equivalence ratios in the three BDGs–air (i.e. GG-H, GG-L, GG-V) premixed flames. A revised mechanism of the GRI-Mech 3.0 is presented through modifying rate coefficients of some key reactions. The behaviors of cell formation of the three BDGs–air flames with and without adding 10%, 20% by volume of each fuel component (i.e. H_2, CO, CH_4) are also discussed. All the experiments were done at room temperature and elevated pressures using the centrally ignited, outwardly propagating spherical flames method. This method yields highly accurate results for both laminar flame speeds and cellular flame instabilities and can easily account for high initial pressures and high initial temperatures [8].

Experimental facility and data analysis

Experimental method

A full, detailed description of the experimental facility is available in Vu et al. [9–11], so only a brief overview is provided here. The total layout of the facility can be seen in Fig. 1. The constant-pressure, outwardly propagating spherical flame was used in this study to collect the experimental data. The internal cylindrical chamber has 220-mm diameter and 220-mm length, with two 100-mm diameter, 40-mm thickness quartz windows mounted on both flat opposite sides of the chamber for flame observation. The reactant mixtures were supplied by adding individual component gases at corresponding partial pressures such that a desired initial chamber pressure could be obtained. The mixtures were centrally ignited by creating a spark across two 0.5-mm diameter electrodes. The propagating spherical flames were imaged using a schlieren system with a 300-W halogen light source and a pair of 150-mm diameter spherical concave mirrors and were recorded using a high-speed digital camera (Phantom v7.2) operated at 10,000 fps. The measurements were restricted to flames with radii larger than 6 mm and smaller than 30 mm to avoid both ignition disturbances and pressure increasing more than 1% of the initial pressure.

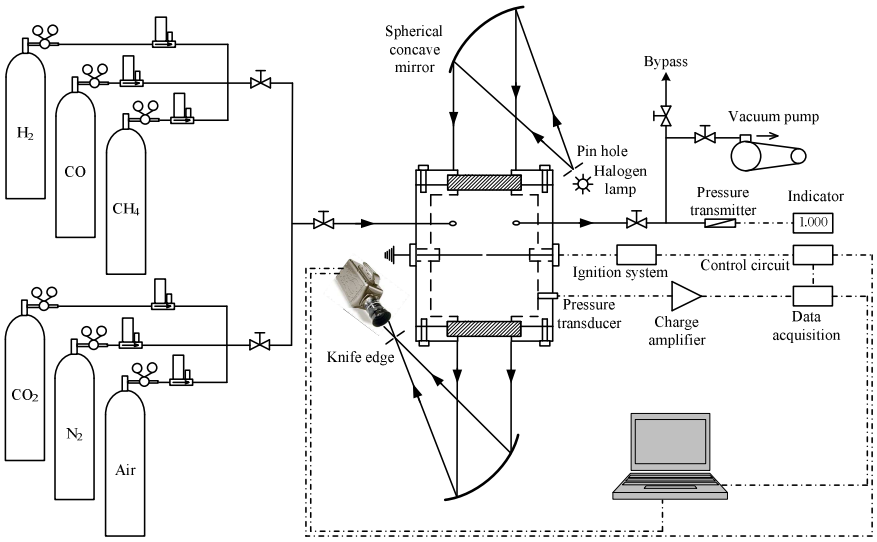

Figure 1. Schematic representation of the experimental setup.

Numerical modeling

In the present study the steady, one-dimensional, laminar premixed flame code PREMIX [12] was used to predict the unstretched laminar burning velocity, which was then compared to experimental data. The GRI-Mech 3.0 mechanism [13], which consists of 53 species and 325 elementary reaction steps, was adopted for the numerical simulations. This model was chosen because it includes all of the species required in this study. However, the GRI-Mech 3.0 is primarily designed to describe methane combustion, therefore it is required to be revised and modified to get a better agreement with the experimental results by replacing rate coefficients in Arrhenius form of some important reactions with ones from several referential reaction mechanisms in literature. The mechanisms referred here are the optimized H_2/CO mechanism of Davis et al. [14], the comprehensive C_1 mechanism of Li et al. [15], the C_1–C_3 model so-called the San Diego mechanism [16], the CO/H_2 mechanism developed by Sun et al. [17], the H_2/CO/C_1–C_4 model, USC Mech Version II, developed by Wang et al. [18], and the mechanism developed by Konnov for small hydrocarbons flames [19].

Laminar burning velocity and Markstein length of biomass derived gases–air calculation

In the present study the constant pressure method was used for the outwardly propagating spherical flame. The detailed calculated process can be found elsewhere [10,11]. The flame front has a propagation velocity $\mathrm{d}R/\mathrm{d}t$, where R is the instantaneous radius of the flame in the schlieren photograph and t is the elapsed time from spark ignition. Flame stretch rate of a spherical flame surface can be expressed as [10,11]

$$K = \frac{1}{A_1}\frac{\mathrm{d}A_1}{\mathrm{d}t} = \frac{2}{R}\frac{\mathrm{d}R}{\mathrm{d}t} \tag{1}$$

where A_1 is the surface area of the flame front. For weakly stretched flames, a linear relationship between the stretched flame speed and the stretch rate exists that is quantified by a burned gas Markstein length, L_b [20,21]

$$S_1 - S_\mathrm{n} = L_\mathrm{b}K \tag{2}$$

where S_1 is the unstretched flame speed with respect to the burned mixture. Base on the plot

of S_n–K from Eq. (2), S_1 can be obtained as the intercept value at $K = 0$ and L_b is the negative value of the slope of the S_n–K line. The unstretched laminar burning velocity with respect to the unburned mixture, S_u^0, is given through mass conservation

$$S_u^0 = S_1\left(\frac{\rho_b}{\rho_u}\right) \tag{3}$$

where ρ_u and ρ_b are densities of the unburned and burned mixtures, respectively.

Important factors for cellular instabilities

The cellular instabilities of the three BDGs–air premixed flames were identified and evaluated with respect to hydrodynamic and diffusional-thermal instabilities. In the present study body-force effect was not significant and could be neglected because the laminar burning velocities of the flames mentioned in this study are large enough such that the flames can overcome the impact of the body-force factor. Initially, cellular instabilities are suppressed by the strong curvature associated with a small flame radius. However, as the flame expands and flame stretch decreases, a state is reached in which the cell development can no longer be suppressed, and cells will appear almost instantaneously over the entire flame surface.

The influences of the hydrodynamic and diffusive-thermal effects were mentioned in detail in Ref. [11]. The hydrodynamic effect is caused by the thermal expansion ratio through the flame front, $\sigma = \rho_u/\rho_b$, and laminar flame thickness, l_f. The laminar flame thickness is a characteristic length scale which is given by Law et al. [22] as $l_f = (\lambda/c_P)/(\rho_u S_u^0)$, where λ and c_P are the thermal conductivity and specific heat at 1200 K, respectively, which is an approximate average of the free stream and flame temperatures [22]. Diffusive-thermal effect is caused by the non-similar diffusion of mass versus heat and are represented by the Lewis number, *Le*, which is defined as a ratio of the heat diffusivity of the mixture to the mass diffusivity of the limiting reactant relative to the abundant inert [20]. The effective Lewis number is defined as the combination of the fuel and oxidizer Lewis numbers [9–11]

$$Le_{eff} = 1 + \frac{(Le_E - 1) + (Le_D - 1)A_2}{1 + A_2} \tag{4}$$

where Le_E, Le_D are the Lewis numbers of excessive and deficient reactants, and A_2 is a measurement of the mixture strength, which were defined in Ref. [9–11]. In case of lean mixture, the Lewis number of the deficient reactant is named fuel Lewis number defined as a weighted average of the Lewis numbers of the three fuels (CO, H_2, CH_4) [9–11,22]

$$Le_F = 1 + \frac{q_{CO}(Le_{CO} - 1) + q_{H_2}(Le_{H_2} - 1) + q_{CH_4}(Le_{CH_4} - 1)}{q} \tag{5}$$

where $Le_{CO}, Le_{H_2}, Le_{CH_4}$ are the fuel Lewis numbers of pure CO–air mixture at ϕ_{CO}, pure H_2–air mixture at ϕ_{H_2}, pure CH_4–air mixture at ϕ_{CH_4}, respectively [9–11]; $q = q_{CO} + q_{H_2} + q_{CH_4}$ is the total heat release, where q_j (j = CO, H_2, CH_4) is the nondimensional heat release associated with the consumption of species j [22].

Results and discussion

Unstretched laminar burning velocities

The measured S_u^0 of the three BDGs–air mixtures at P_u = 0.1 MPa as a function of equivalence ratio are plotted in Fig. 2. Together with the results from the present work, the S_u^0 of the $50H_2$:50CO–air flames and the $5H_2$:95CO–air flames by McLean et al. [23] are also shown in the same figure. It is clear from Fig. 2 that the GG-V–air flames have the highest burning velocity compared to those of the two other mixtures because of the highest H_2 content in the GG-V mixture. Next, because of the higher ratio of H_2/CO concentrations in the mixture of GG-L compared to one of GG-H, it demonstrates a higher S_u^0 of the GG-L–air flames compared to those of the GG-H–air flames, (the ratios of H_2/CO/CO_2 are 1.18/0.93/1 and 1.06/1.31/1 for GG-L and GG-H respectively). The maximum S_u^0 of all three BDGs–air premixed flames were found at ϕ = 1.4 (i.e. 73.05 cm/s, 80.64 cm/s, and 135.25 cm/s for the GG-H–air, the GG-L–air, and the GG-V–air flames, respectively). In discussing the location of the peak burning velocity, reference to the two dashed line in Fig. 2 would indicate that the S_u^0 of the $50H_2$:50CO–air flames and the $5H_2$:95CO–air flames respectively have the peaks at ϕ = 2.5 and ϕ = 2, also literature shows that H_2–air flames have the maximum S_u^0 at ϕ = 1.4 [24] and CH_4–air flames have the peak S_u^0 at ϕ = 1.1 [25]. The GG-V mixture has H_2:CO = 3:1, hence the peak burning velocity may be at ϕ between 1.4 and 2.0; with the existence of CH_4 in the mixture, the peak has to shift to lower ϕ (i.e. ϕ = 1.4 here). The GG-H has H_2:CO = 0.8:1 causing the peak burning velocity at ϕ a little higher than 2.0, while the GG-L has H_2:CO = 1.27:1 inducing the peak burning velocity at ϕ a little lower than 2.0, but the high percentages in CO_2 dilution make the decrease of thermal diffusivity in the reactant mixtures [26], therefore the burning peaks tend to shift to lower equivalence ratio (i.e. ϕ = 1.4 here).

Sensitivity analysis

As mentioned above, the PREMIX code [12] and the GRI-Mech 3.0 mechanism [13] were used for the prediction of burning velocities. As shown in Fig. 3, the experimental measurements and predictions for S_u^0 agree well at lean and stoichiometric flames, but they diverge much at rich flames. As an effort to identify the dominant reactions in the GRI-Mech 3.0 that lead to the observed differences at rich flames, a sensitivity analysis with respect to the reaction rate coefficients was performed for the three BDGs–air premixed flames. In this study, the first-order normalized sensitivity coefficient of a given species affected by a certain reaction is defined as a relative value equaling the quotient of the sensitivity coefficient of

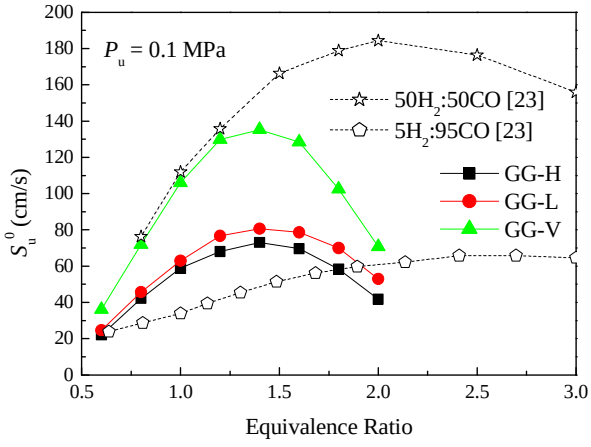

Figure 2. Unstretched laminar burning velocities of the three BDGs–air premixed flames at P_u = 0.1 MPa, together with data of $50H_2$:50CO–air and $5H_2$:95CO–air by McLean et al. [23].

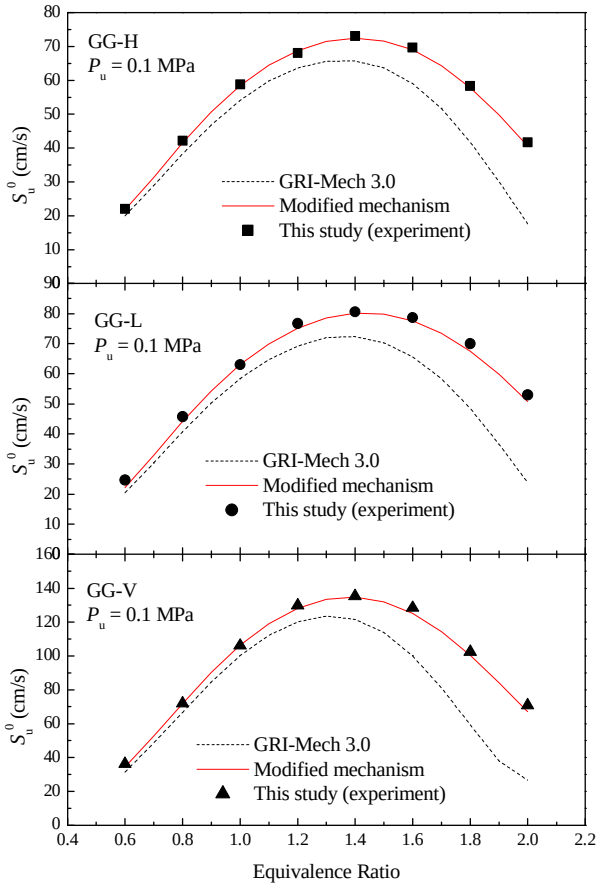

Figure 3. Experimental (points), calculated by GRI-Mech 3.0 (dashed lines), and calculated by revised mechanism (solid lines) S_u^0 of the three BDGs–air flames at P_u = 0.1 MPa.

that reaction and the sensitivity coefficient of the most sensitive reaction, which holds the largest sensitivity coefficient. This definition can be applied to compute the normalized sensitivity coefficients of the three fuel species (i.e. CH_4, H_2, CO) of the BDGs used in this study and only the relative values larger than +0.1 or smaller than –0.1 are reported here. Fig. 4 demonstrates the first-order normalized sensitivity coefficient of CH_4 species at P_u = 0.1 MPa, ϕ = 1.5 for the 21 elementary reactions exhibiting the largest sensitivities based on the GRI-Mech 3.0 mechanism, which emphasizes results at fuel-rich conditions where the discrepancies between measurements and predictions are large. Similarly, the normalized sensitivity coefficients of H_2 and CO species of the GG-H–air flames at P_u = 0.1 MPa, ϕ = 1.5 for the seven reactions exhibiting the largest sensitivities are presented in Fig. 5. A positive sensitivity coefficient indicates that increasing the reaction rate coefficient increases burning velocity; conversely, a negative sensitivity coefficient means that increasing the reaction rate coefficient decreases burning velocity. Therefore, in order to get a better agreement between measured and predicted S_u^0 at fuel-rich conditions, the GRI-Mech 3.0 mechanism were revised by replacing the reaction rate coefficients of these sensitive reactions by ones from referential reaction mechanisms until reaching a best fit between predicted S_u^0 and our experimental data. The modified parameters of pre-exponential factor A, power of n, activation energy E_a were collected from the kinetic data for combustion modeling in literature [14–19] and are listed in Table 2.

As can be seen in Fig. 3, the experimentally measured S_u^0 of the three BDGs–air premixed flames get better agreement with the prediction values obtained by the revised

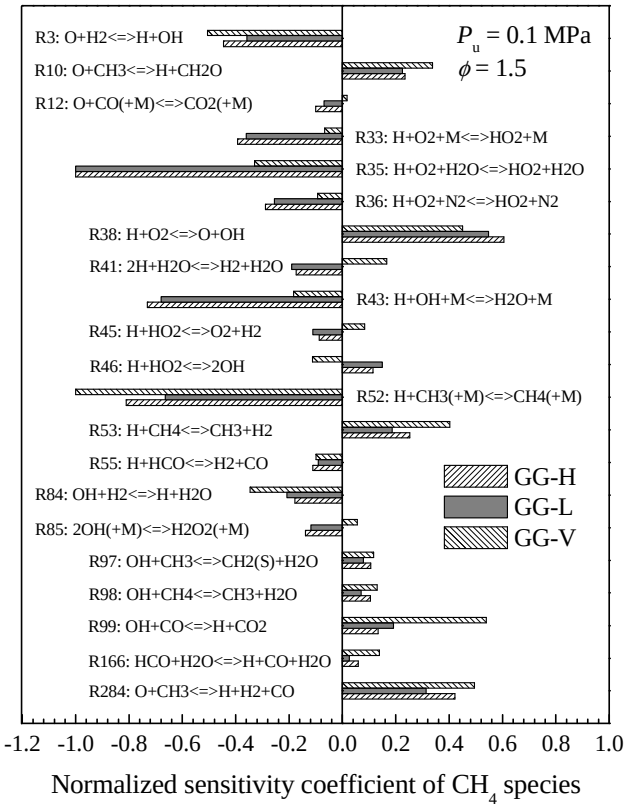

Figure 4. First-order normalized sensitivity coefficient of CH_4 species of the three BDGs–air premixed flames at ϕ=1.5, P_u = 0.1 MPa.

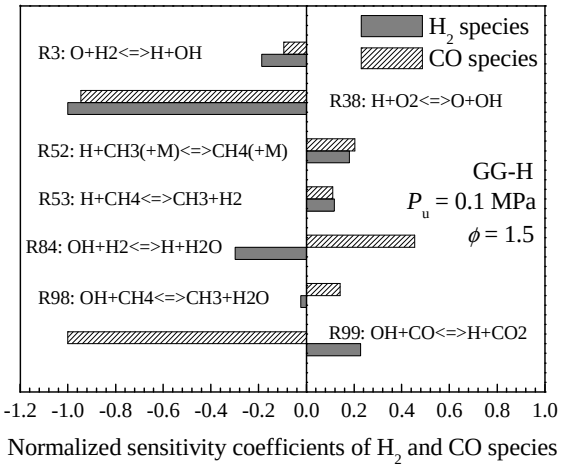

Figure 5. First-order normalized sensitivity coefficient of H_2 and CO species of the three BDGs–air premixed flames at ϕ=1.5, P_u = 0.1 MPa.

mechanism, even at fuel-rich flames. It is shown that the largest discrepancy between them is about 3 cm/s. The maximum S_u^0 of the three BDGs–air premixed flames by predicting using the revised mechanism occur at equivalence ratio of 1.4, matching with the peak burning velocities of experimental data.

Markstein lengths

The negative value of the slope of the straight-line fit between stretched flame speed and flame stretch rate is defined as the burned gas Markstein length, L_b, which represents the influence of the flame speed on the flame stretch rate. The L_b varies with the difference equivalence ratios, mixture compositions and initial pressures. For the case of a negative L_b, the flame speed increases along with an increase in the flame stretch rate. In this case, if any protuberance occurs on the flame front, then the flame speed increases, leading to the enhanced flame instability. On the other hand, if $L_b > 0$, the flame-front instabilities are suppressed, thereby contributing to the flame stabilization [21,25]. Fig. 6 plots the measured L_b of the three BDGs–air premixed flames as a function of equivalence ratio at the initial pressure of 0.1 MPa. This figure indicates that the L_b of all mixtures are smaller than zero; therefore such mixtures are unstable to flame stretch effects. For all measured BDGs–air mixtures, L_b increase along with equivalence ratio as shown in Fig. 6. This tendency is similar to the tendencies of L_b of the $50H_2$:50CO–air flames [26] and the CH_4–air flames [25]. The L_b of the GG-H–air flames and the GG-L–air flames are lower than those of the GG-V–air flames, because of the high CO_2 concentrations in the GG-H and the GG-L mixtures, causing the significant decrease in the L_b of the mixtures [10,26].

Table 2. Reaction rate coefficients in Arrhenius form $k = AT^n \exp(-E_a/R^0T)$. Units are mole-cm-s-cal-K.

No.	Name	Reaction	*A*	*n*	E_a	Ref.
1	R3	O+H2<=>H+OH	3.820E+12	0.000	7948.00	[17]
2	R10	O+CH3<=>H+CH2O	8.430E+13	0.000	0.00	[15,16,18,19]
3	R38	H+O2<=>O+OH	3.547E+15	–0.406	16599.00	[15]
4	R41	2H+H2O<=>H2+H2O	5.624E+19	–1.250	0.00	[14,18]
5	R45	H+HO2<=>O2+H2	1.660E+13	0.000	823.00	[15,16]
6	R46	H+HO2<=>2OH	1.700E+14	0.000	875.00	[19]
7	R52	H+CH3(+M)<=>CH4(+M)	1.270E+16	–0.630	383.00	[15,16,18]
8	R53	H+CH4<=>CH3+H2	5.470E+07	1.970	11210.00	[15]
9	R55	H+HCO<=>H2+CO	5.000E+13	0.000	0.00	[16]
10	R84	OH+H2<=>H+H2O	1.170E+09	1.300	3635.28	[16]
11	R98	OH+CH4<=>CH3+H2O	5.720E+06	1.960	2639.00	[15]
12	R166	HCO+H2O<=>H+CO+H2O	2.244E+18	–1.000	17000.00	[14,18]

Flame stability and cellular structure

In premixed flames, a corrugated flame front due to the formation of cellular instabilities could induce the turbulence of unburned mixture and subsequently the rapid increase of flame propagation velocity, hence could be one of the main reasons for gas explosion. As previously mentioned, two instabilities of premixed flame were observed in this study: diffusional-thermal instability and hydrodynamic instability. In order to compare the cellularity behavior of the three BDGs–air premixed flames, schlieren images of different sequences of the GG-H–air flames, the GG-L–air flames, and the GG-V–air flames for equivalence ratio of 0.8 are shown at P_u = 0.2 MPa in Fig. 7a and at P_u = 0.3 MPa in Fig. 7b for the same Karlovitz number, which is the non-dimensional measure of stretched rate and can be defined as a ratio of chemical time scale, which is represented by the ratio of flame thickness to flame speed, and physical time scale, which is given by the inverse of flame stretch, $Ka = (2/R)(\mathrm{d}R/\mathrm{d}t)/(S_u^0/l_f)$ [8]. Three important parameters (Le_{eff}, σ, l_f), which affect the

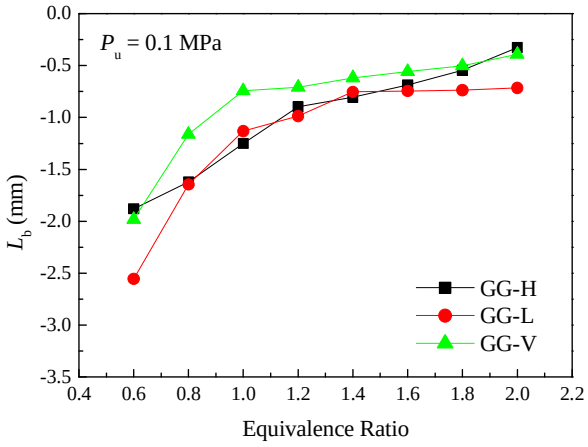

Figure 6. Markstein lengths of the three BDGs–air premixed flames at P_u = 0.1 MPa for a wide range of equivalence ratios.

cellularity of the flames, are tabulated at the bottom of the figure. This figure exhibits that the flame fronts behavior of the GG-H–air flames and the GG-L–air flames are quite similar, while the GG-V–air flames are more wrinkled on the flame surfaces. For the GG-H–air flames and the GG-L–air flames, the Le_{eff} are equal, causing no different effect on the diffusional-thermal instability. Concerning the hydrodynamic instability, the σ and the l_{f} change a little, hence causing a slight influence on the hydrodynamic effect. For the GG-V–air flames, compared to the GG-H–air flames and the GG-L–air flames, the σ increases, and the l_{f} significantly decreases; thus the effect of the hydrodynamic instability would be promoted. In addition, the Le_{eff} is much lower than those of the GG-H–air flames and the GG-L–air flames; therefore the flame front instabilities of the GG-V–air flames can be enhanced. It is clear from Fig. 7a and b that different initial pressures cause different sequences of the flames, cells form earlier and the size of cells is smaller at higher P_{u}. The Le_{eff} is insensitive to initial pressure changes; therefore the propensity to destabilize the flames was not affected by the diffusive-thermal effect. The enhancement of cellularity at higher P_{u} could be explained by the significant decrease in the l_{f}, whereas the σ maintains nearly the same value.

In discussing the effects of each fuel component in mixtures, flame sequences are evaluated by increasing the concentration of each fuel in the reactant mixtures. For hydrogen enrichment, Fig. 8 indicates that the propensity of destabilization tends to be progressively promoted. It is noteworthy to mention that the σ does not change so much while the l_{f} decreases significantly causing the enhancement in hydrodynamic effect. Additionally, the Le_{eff} of the flame decreases with adding of H_2 content hence intensifies the diffusive-thermal effect. It can be concluded that both the hydrodynamic instability and diffusional-thermal instability are promoted when the amount of hydrogen increases in the reactant mixtures.

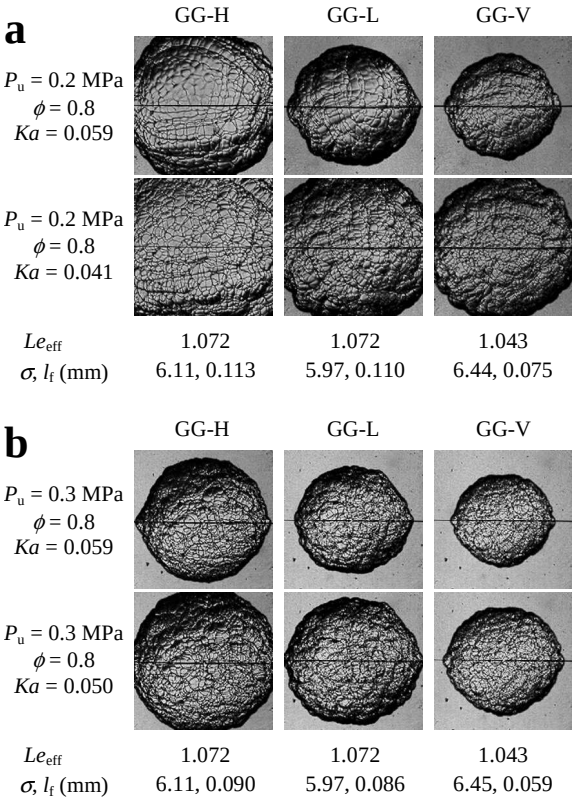

Figure 7. Schlieren images of the three BDGs–air premixed flames at ϕ = 0.8, (a) P_{u} = 0.2 MPa and (b) P_{u} = 0.3 MPa.

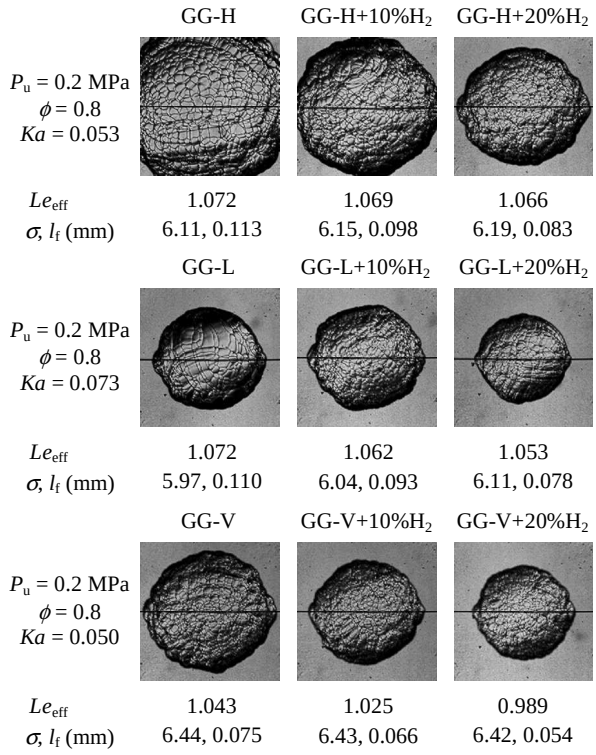

Figure 8. Schlieren images of the three BDGs–air premixed flames with H_2 enrichment at ϕ = 0.8, P_{u} = 0.2 MPa.

Regarding to effects of CO addition, Fig. 9 shows that there are no differences in sequences of the flame front surfaces between the BDGs–air premixed flames with and without CO additions. As increasing content of CO in the reactant mixtures, the Le_{eff} slightly increases, thereby the diffusional-thermal instability would be slightly diminished. Meanwhile, the hydrodynamic instability would be a little promoted because of a small increase in the σ and a slight decrease in the l_f. Hence the net effects of the two instabilities can be negligible. The combination of the diffusional-thermal instability and the hydrodynamic instability indicates that increasing CO concentration in the fuel blends could not suppress the cellular instabilities of the BDGs–air flames.

The effects of methane additions on cellularity of the BDGs–air flames are illustrated in Fig. 10. It is different from the cases in the $50H_2$:50CO syngas–air premixed flames that could not be suppressed by methane additions [9,11], herein the flame front instabilities are diminished as the amount of methane addition in the fuel blend increases. The most suitable parameter that denotes the stabilizations in the BDGs–air flames with CH_4 additions is the significant increase in the l_f. For methane addition, the Le_{eff} decreases, causing an enhancement in diffusional-thermal instability. The σ increases, however the l_f progressively increases, and these thus suppress hydrodynamic instability. It indicates that l_f can be the dominant factor as the suppressant or in the enhancement flame front instabilities. It also demonstrates that the hydrodynamic effect is the main factor when the flame has a large size, while the diffusive-thermal effect is only dominant at the time when flame is ignited and has a small size [8]. Compared to the GG-H–air flames and the GG-L–air flames, the GG-V–air flames is not so much suppressed by CH_4 addition, and this tendency is similar to the behaviors of the CH_4-added $50H_2$:50CO syngas–air flames [9,11]. Because both flames have high burning velocities and thereby small flame thicknesses, therefore the increase in flame thickness could not significantly affect the cellularity of the flames.

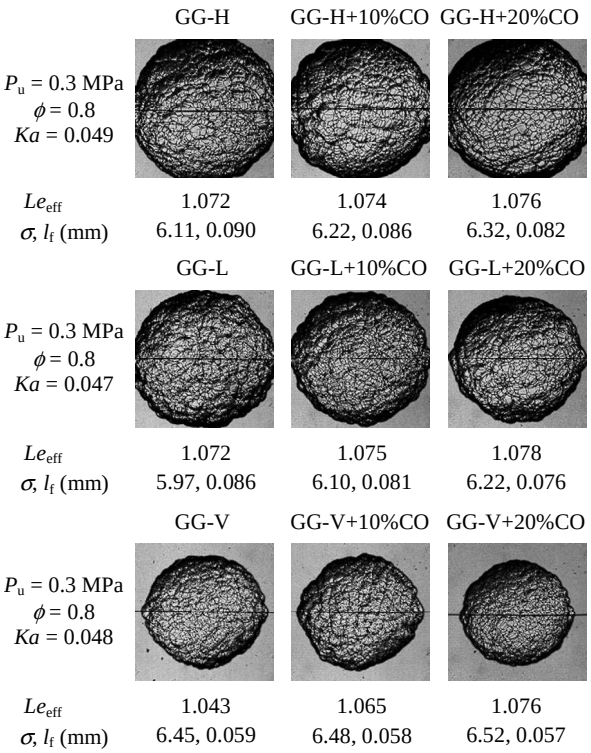

Figure 9. Schlieren images of the three BDGs–air premixed flames with CO addition at ϕ = 0.8, P_u = 0.3 MPa.

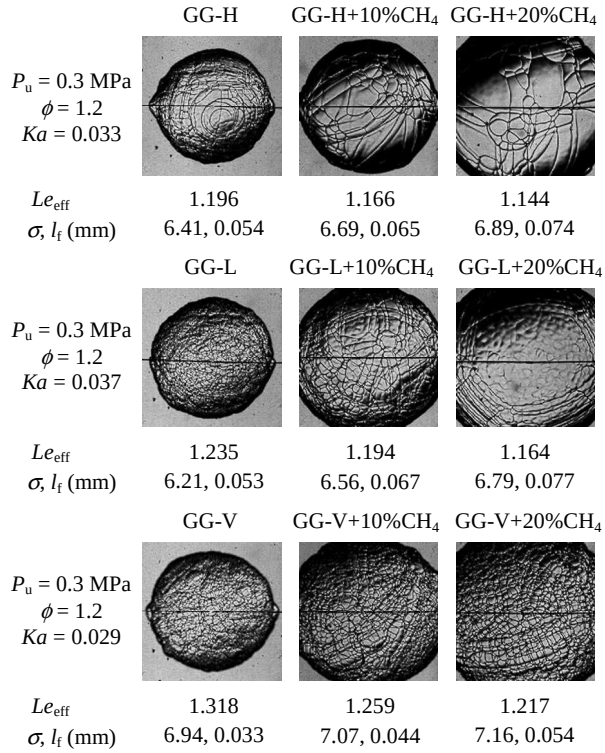

Figure 10. Schlieren images of the three BDGs–air premixed flames with CH_4 addition at ϕ = 1.2, P_u = 0.3 MPa.

Conclusions

The major conclusions of the study are as follows:

The S_u^0 of the GG-V–air flames are higher than those of the GG-L–air flames and the GG-H–air flames and the peak burning velocities of the three BDGs–air premixed flames were found at equivalence ratio of 1.4. The experimental measurements and predictions using GRI-Mech 3.0 of S_u^0 agree well at lean and stoichiometric flames, but they diverge much at rich flames. For getting a better agreement between the measured and predicted burning velocities at fuel-rich conditions, sensitivity analysis was performed to identify the dominant reactions. Subsequently the rate coefficients of these important reactions were replaced by ones from referential reaction mechanisms in literature. The new calculated burning velocities from the revised mechanism agree rather well with the experimental data. The L_b of the three BDGs–air premixed flames are smaller than zero, thereby the flames are sensitive to flame stretch effects and the L_b increase with equivalence ratio.

The flame front behaviors of the GG-H–air flames and the GG-L–air flames are quite similar, while the GG-V–air flames are more wrinkled on the flame surfaces because of the combined influences of the hydrodynamic and the diffusional-thermal instabilities. For hydrogen enrichment, the propensity of destabilization tends to be progressively promoted because of the enhancement on both effects. For carbon monoxide addition, there are no differences in sequences of the flame front surfaces between the BDGs–air premixed flames with and without carbon monoxide additions. For methane additions, the flame front instabilities are diminished because of the significant increase in the flame thickness.

Acknowledgements

This work was supported by the cooperation business between Korea Gas Corporation and Pukyong National University in 2010-11.

References

[1] Yan, B., Wu, Y., Liu, C., Yu, J.F., Li, B., Li, Z.S., et al., “Experimental and modeling study of laminar burning velocity of biomass derived gases/air mixtures”, *Int. J. Hydrogen Energy* 36:3769–3777 (2011).

[2] Liu, C., Yan, B., Chen, G., Bai, X.S., “Structures and burning velocity of biomass derived gas flames”, *Int. J. Hydrogen Energy* 35:542–555 (2010).

[3] Hanaoka, T., Inoue, S., Uno, S., Ogi, T., Minowa, T., “Effect of woody biomass components on air–steam gasification”, *Biomass Bioenergy* 28:69–76 (2005).

[4] Lv, P., Yuan, Z., Ma, L., Wu, C., Chen, Y., Zhu, J., “Hydrogen-rich gas production from biomass air and oxygen/steam gasification in a downdraft gasifier”, *Renew. Energy* 32:2173–2185 (2007).

[5] Valliyappan, T., Ferdous, D., Bakhshi, N.N., Dalai, A.K., “Production of hydrogen and syngas via steam gasification of glycerol in a fixed-bed reactor”, *Top. Catal.* 49:59–67 (2008).

[6] Williams, F.A., *Combustion theory*, 2nd ed. Redwood City, CA:Addison-Wesley, 1985. p. 349.

[7] Kadowaki, S., Suzuki, H., Kobayashi, H., “The unstable behavior of cellular premixed flames induced by intrinsic instability”, *Proc. Combust. Inst.* 30:169–176 (2005).

[8] Law, C.K., Kwon, O.C., “Effects of hydrocarbon substitution on atmospheric hydrogen–air flame propagation”, *Int. J. Hydrogen Energy* 29:867–879 (2004).

[9] Vu, T.M., Park, J., Kwon, O.B., Kim, J.S., “Effects of hydrocarbon addition on cellular instabilities in expanding syngas–air spherical premixed flames”, *Int. J. Hydrogen Energy* 34:6961–6969 (2009).

[10] Vu, T.M., Park, J., Kwon, O.B., Bae, D.S., Yun, J.H., Keel, S.I., “Effects of diluents on cellular instabilities in outwardly propagating spherical syngas–air premixed flames”, *Int. J. Hydrogen Energy* 35:3868–3880 (2010).
[11] Vu, T.M., Park, J., Kim, J.S., Kwon, O.B., Yun, J.H., Keel, S.I., “Experimental study on cellular instabilities in hydrocarbon/hydrogen/carbon monoxide–air premixed flames”, *Int. J. Hydrogen Energy* 36:6914–6924 (2011).
[12] Kee, R.J., Grcar, J.F., Smooke, M.D., Miller, J.A., “A Fortran program for modeling steady laminar one-dimensional premixed flames”, Report No. SAND85-8240, Sandia National Laboratories, 1993.
[13] Smith, G.P., Golden, D.M., Frenklach, M., Moriarty, N.W., Eiteneer, B., Goldenberg, M., et al., “GRI-Mech 3.0”, http://www.me.berkeley.edu/gri_mech/.
[14] Davis, S.G., Joshi, A.V., Wang, H., Egolfopoulos, F., “An optimized kinetic model of H_2/CO combustion”, *Proc. Combust. Inst.* 30:1283–1292 (2005).
[15] Li, J., Zhao, Z., Kazakov, A., Chaos, M., Dryer, F.L., Scire, J.J., “A comprehensive kinetic mechanism for CO, CH_2O, and CH_3OH combustion”, *Int. J. Chem. Kinet.* 39:109–136 (2007).
[16] Saxena, P., Williams, F.A., “Testing a small detailed chemical-kinetic mechanism for the combustion of hydrogen and carbon monoxide”, *Combust. Flame* 145:316–323 (2006). http://maeweb.ucsd.edu/combustion/cermech/.
[17] Sun, H., Yang, S.I., Jomaas, G., Law, C.K., “High-pressure laminar flame speeds and kinetic modeling of carbon monoxide/hydrogen combustion”, *Proc. Combust. Inst.* 31:439–446 (2007).
[18] Wang, H., You, X., Joshi, A.V., Davis, S.G., Laskin, A., Egolfopoulos, F., Law, C.K., “USC Mech Version II. High temperature combustion reaction model of H_2/CO/C_1–C_4 compounds”. http://ignis.usc.edu/USC_Mech_II.htm.
[19] Konnov, A.A., “Detailed reaction mechanism for small hydrocarbons combustion”, Release 0.5, 2000. http://homepages.vub.ac.be/~akonnov/.
[20] Clavin, P., “Dynamic behavior of premixed flame fronts in laminar and turbulent flows”, *Prog. Energy Combust. Sci.* 11:1–59 (1985).
[21] Bradley, D., Gaskell, P.H., Gu, X.J., “Burning velocities, Markstein lengths, and flame quenching for spherical methane–air flames: a computational study”, *Combust. Flame* 104:176–198 (1996).
[22] Law, C.K., Jomaas, G., Bechtold, J.K., “Cellular instabilities of expanding hydrogen/propane spherical flames at elevated pressures: theory and experiment”, *Proc. Combust. Inst.* 30:159–167 (2005).
[23] McLean, I., Smith, D.B., Taylor, S.C., “The use of carbon monoxide/hydrogen burning velocities to examine the rate of the CO+OH reaction”, *Proc. Combust. Inst.* 25:749–757 (1994).
[24] Dowdy, D.R., Smith, D.B., Taylor, S.C., “The use of expanding spherical flames to determine burning velocities and stretch effects in hydrogen/air mixtures”, *Proc. Combust. Inst.* 23:325–332 (1990).
[25] Gu, X.J., Haq, M.Z., Lawes, M., Woolley, R., “Laminar burning velocity and Markstein lengths of methane–air mixtures”, *Combust. Flame* 121:41–58 (2000).
[26] Prathap, C., Ray, A., Ravi, M.R., “Investigation of nitrogen dilution effects on the laminar burning velocity and flame stability of syngas fuel at atmospheric condition”, *Combust. Flame* 155:145–160 (2008).